Chapter 7

Microscopic Particle Manipulation via Optoelectronic Devices

Xiaolu Zhu and Yifei Yang

Additional information is available at the end of the chapter

http://dx.doi.org/10.5772/67928

Abstract

The optoelectronic tweezers (or optically induced dielectrophoresis (DEP)) have showed the ability to parallelly position a large number of colloidal microparticles without any template. The microparticles can be trapped and driven by the dielectrophoretic forces induced by the optical micropatterns in OET devices. In this chapter, the design and fabrication of flat optoelectronic devices (FOD) and hybrid optoelectronic device (HOD) are described. In the typical FOD, the manipulation modes including filtering, transporting, concentrating and focusing controlling regimes are experimentally demonstrated and analyzed. The controllable rotation of self-assembled microparticle chains in FOD has also been investigated, and a method incorporating the optically induced electrorotation (OER) and AC electroosmotic (ACEO) effects is numerically and experimentally implemented for manipulating microparticle chains. Based on the above research of FOD, a hybrid DEP microdevice HOD is conceptually and experimentally proposed. The HOD integrates with metallic microelectrode layer and the underneath photoconductive layer with projected optical virtual electrodes. FOD and HOD hybrid device enables the active driving, large-scale patterning and local position adjustment of microparticles. These techniques make up the shortcoming of low flexibility of traditional metallic microelectrodes and integrate the merits of both the metal electrode-induced and microimage-induced DEP techniques.

Keywords: optoelectronic device, dielectrophoresis, optically induced electrorotation, AC electroosmosis

1. Introduction

The manipulation technique based on dielectrophoresis (DEP) [1–3] is easy-to-use and requires no moving parts, thus can achieve massively paralleled and non-contact manipulation for

particles or cells [4, 5]. It is becoming an important enabling technology in filtering [6–8], concentrating [9–11], transporting [12–14] and flow focusing [15, 16] for microparticles. However, these DEP technologies require design and fabrication of sophisticated electrode structures, which lack flexibility and could not provide real-time alterable electrode-patterns for diverse manipulations. Therefore, how to improve the electrodes' flexibility and reconfigurability has become the key concern in the extended application of DEP. The proposal of optically induced DEP (ODEP) [17, 18] based on photoconductive effect in an optoelectronic device offered a potential option for the design of highly flexible and real-time reconfigurable optical microelectrodes. ODEP-based optoelectronic device offers more opportunity to develop miscellaneous particle manipulating techniques in biomedical microsystems, although ODEP device could not fully supersede the traditional physical electrode array.

Usually, the sample pretreatment process in microfluidic analysis system should include functional units capable of filtering, concentrating, transporting and focusing microparticles to be applicable to different sample handing requirements [9, 19, 20]. Filtration is essentially a separation technology, such as the insulative DEP approach for particle separation [21] and the DEP method for characterizing and distinguish stem cells [6]. Once the target particles are isolated after the filtration or separation, the concentration of the target particle population is sometimes low and requires the concentrating steps for the following detection. By now various DEP concentrations of viruses, bacteria have been reported in the literature [22–24]. The function of transporting microparticles nearly runs through the whole process in the microanalysis system, and biological/chemical applications [14, 25–27]. Besides, as an important approach for the continuous single-particle detection and counting, focusing particles into a straight line are also applied in microfluidic devices. The hydrodynamic forces [28, 29] and electrokinetic force [30, 31] are usually employed to realize flow focusing. However, the above sample handling approaches require fabricating complex multi-functional electrode array or structures to achieve versatile manipulation of the micro/nano bio-particles, and the previous work also has difficulties in providing real-time alterable electrode patterns to accommodate different manipulation requirements. So, the promotion of DEP technology in the application of the micro/nano manipulation faces some restrictions. In recent years, Chiou et al. [18, 32] reported parallel manipulation of single particles using a variant of DEP mechanism—ODEP mechanism which offers the ability to trap single particles parallelly and massively. ODEP has also been used to discriminate normal oocytes at a certain frequency [33]. However, the manipulation regimes still need more systematic study. Therefore, this chapter will experimentally verify and analyze the optical pattern and controlling regimes for filtering, transporting, concentrating and focusing based on ODEP.

In addition to the above manipulation modes for microparticle or cells, the ODEP-based optoelectronic device could serve as a more powerful tool to spatially manipulate and regulate the posture, orientation and position of microparticle chains or other microstructures. The previous methods for manipulating micro-objects usually need templates, physical or chemical reaction process involving more extra techniques [34]. Many of the created particle chains or closely linked chains are immobilized, and their relative positions cannot be stably controlled. The ODEP (also called optoelectronic tweezers, OETs) has showed the ability to parallelly

http://dx.doi.org/10.5772/67928

position colloidal particles without any template [18, 35]. The microparticles can be trapped and driven by the DEP forces induced by the optical micropatterns in optoelectronic devices [36, 37]. However, the rotation of assembled microparticle chains by OETs has rarely been investigated, and the degree of freedom for varying the postures, positions or orientations of the microparticle chains still has limitations. To demonstrate the promoted ability of optoelectronic devices, this chapter will experimentally demonstrate the method incorporating optically induced electrorotation (OER) and alternating current electroosmotic (ACEO) effects, for the formation and motion control of microparticle chains.

By comprehensively analyzing the traditional physical electrode array and ODEP-based optoelectronic device, we further developed a hybrid optoelectronic device (HOD) that could integrate the merits of both the traditional physical electrode array and ODEP-based optoelectronic device. The ODEP-based optoelectronic device offers a flexible and real-time dynamic manipulating scheme but needs more external optic devices; the traditional physical electrode array offers a more stable working status and higher integration but lack the ability of real-time particle manipulation. In Section 5 of this chapter, HOD is conceptually proposed, and its prototype is designed and fabricated. This type of hybrid device enables the active driving, large-scale patterning and locally position adjustment of microparticles.

2. Design and fabrication of optoelectronic devices

2.1. The design and fabrication of flat optoelectronic devices

The flat optoelectronic devices (FOD) consisted of several layers, including indium tin oxide (ITO) and photoconductive layers. To fabricate photoconductive layer of FOD chip (as shown in **Figure 1(a)**), 50-nm doped hydrogenated amorphous silicon (n + *a*-Si:H), 1.5-μm intrinsic *a*-Si:H and 25-nm silicon carbide (SiC*x*) passivation layer were consecutively deposited by plasma-enhanced chemical vapor deposition (PECVD) method on the bottom ITO-coated glass at 200°C. The n+ *a*-Si:H was deposited from a gas ratio of 1% PH_3 in SiH_4, and then, the intrinsic *a*-Si:H was deposited from a gas mixture containing SiH_4 and H_2. Afterwards, the

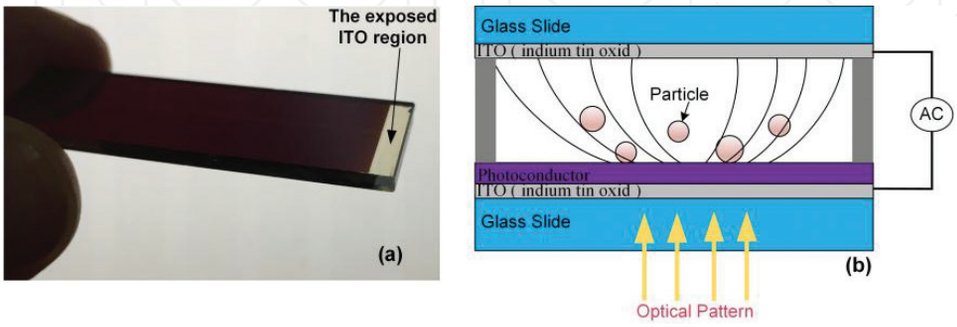

Figure 1. Schematic diagram of the FOD chip based on ODEP mechanism. (a) Photograph of the photoconductive substrate; (b) structure diagram of the ODEP microdevice.

SiC*x* layer was deposited by a SiH_4, CH_3 and N_2 mixture. After that, the ITO layer for bias connections was exposed via reactive ion etch (RIE), as shown in **Figure 1a**. The photoconductive layer of the microdevice consisted of n +*a*-Si:H layer, intrinsic *a*-Si:H layer and SiC*x* layer (as shown in **Figure 1b**). The n + *a*-Si:H layer was used as both a transitionary and adhesive layer from the intrinsic *a*-Si:H layer to the bottom ITO-coated glass. During chip packaging, firstly, a double-faced adhesive tape with a thickness of ~ 100μm was pasted on the four edges of the photoconductive surface to form a microchamber with a scale of ~15 mm × 8 mm. Then a droplet containing microsphere particles was dripped into the microchamber using a pipette. Lastly, the top ITO-glass slide was placed onto the roof of the microchamber to make the microchamber sealed as shown in **Figure 1b**. In the whole ODEP device, a 100-μm insulating spacer was used to maintain the gap between the upper ITO film and lower photoconductive layer (see **Figure 1b**). The alternating current (AC) voltage was supplied between the top and bottom ITO layers.

For the fabricated FOD chip as shown in **Figure 1**, the photoconductor has a high electric impedance (about 1×10^{-6} S/m, for example) prior to illumination, so at this time the majority of the applied voltage drops across the photoconductive layer, which causes a weak, uniform electric field inside the liquid layer. At this state, no ODEP force generates. When a projected light source hits the amorphous silicon layer (photoconductive layer), electron-hole pairs are excited, thus decreasing the impedance of the photoconductive layer by thousands of times (~5000 times, for example), and the electrical conductivity of the photoconductor increases to ~5×10^{-3} S/m. At this state, the virtual electrodes are formed in the photoconductor, and the voltage drop across the liquid layer in the illuminated area is much higher than that in the dark area. Consequently, the bright-dark pattern induces a non-uniform electric field inside this device. The dense electric filed lines appear at the illuminated areas, and the sparse field lines appear at the dark areas as shown in **Figure 1b**. Thus, a DEP force acting on microparticles can be induced in the liquid chamber(or called fluidic chamber), and the time-averaged DEP force acting on the spherical microparticle suspended inside liquid chamber can be mathematically described as follows [38]

$$\langle \mathbf{F}_{\mathrm{DEP}} \rangle = \pi R^3 \varepsilon_{\mathrm{m}} \mathrm{Re}\left[\frac{\tilde{\varepsilon}_{\mathrm{p}} - \tilde{\varepsilon}_{\mathrm{m}}}{\tilde{\varepsilon}_{\mathrm{p}} + 2\tilde{\varepsilon}_{\mathrm{m}}}\right] \nabla E^2 \tag{1}$$

where R is the particle radius, E is the amplitude of electric field, $\tilde{\varepsilon}_{\mathrm{p}}$ and $\tilde{\varepsilon}_{\mathrm{m}}$ are the complex permittivities of the microparticle and suspending medium, respectively, $\tilde{\varepsilon}_{\mathrm{p}} = \varepsilon_{\mathrm{p}} - j\sigma_{\mathrm{p}}/\omega$, and $\tilde{\varepsilon}_{\mathrm{m}} = \varepsilon_{\mathrm{m}} - j\sigma_{\mathrm{m}}/\omega$. Here, σ_{p} and σ_{m} are ohmic electrical conductivities of the microparticle and liquid medium, respectively; ε_{p} and ε_{m} are the permittivities of the microparticle and liquid medium; ω is angular frequency of the electric field or the applied AC voltage. In Eq. (1), the expression in brackets (i.e., $(\tilde{\varepsilon}_{\mathrm{p}} - \tilde{\varepsilon}_{\mathrm{m}})/(\tilde{\varepsilon}_{\mathrm{p}} + 2\tilde{\varepsilon}_{\mathrm{m}})$) is referred to as the Clausius-Mossotti (CM) factor that is denoted as f_{CM}. When $\mathrm{Re}[f_{CM}] > 0$, positive DEP occurs and particles move toward high field regions; when $\mathrm{Re}[f_{CM}] < 0$, negative DEP occurs and particles move toward weak field regions. The particles in solution also undergo the opposing Stokes' drag [39], as follows

$$\boldsymbol{F}_{\mathrm{drag}} = -6\pi\eta RV \tag{2}$$

where V is the particle velocity, and η is the dynamic viscosity of the liquid.

http://dx.doi.org/10.5772/67928

2.2. The design and fabrication of hybrid optoelectronic device (HOD)

The hybrid optoelectronic device (HOD) has a more compact structure, integrating another layer of physical electrode array above the photoconductive layer. In another word, the HOD (several cm^2) integrates with photoconductive layer and metal microelectrodes including the quadrupole electrodes and spiral electrodes as shown in **Figures 2** and **3**. **Figure 2** is the schematic design diagram of this microdevice. This HOD has a hamburger-like structure. The upper plate was transparent ITO conductive glass. The lower plate included the photoconductive layer (or called photoconductor) and the bottom glass slide. The photoconductive *a*-Si:H layer was on the bottom ITO film, and the insulating silicon nitride (or silicon carbide)

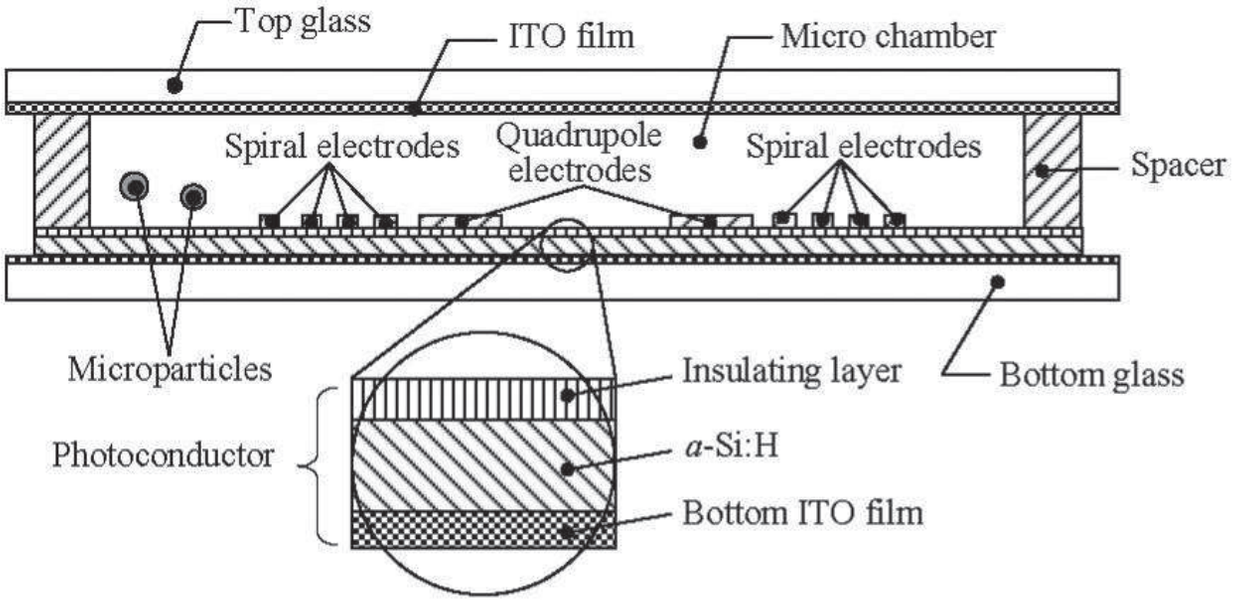

Figure 2. Schematic representation of HOD cross section along the line of AA′ in **Figure 3**. The photoconductor consists of insulating layer, *a*-Si:H layer and the bottom ITO film. Only a few representative electrodes are drawn for simplicity.

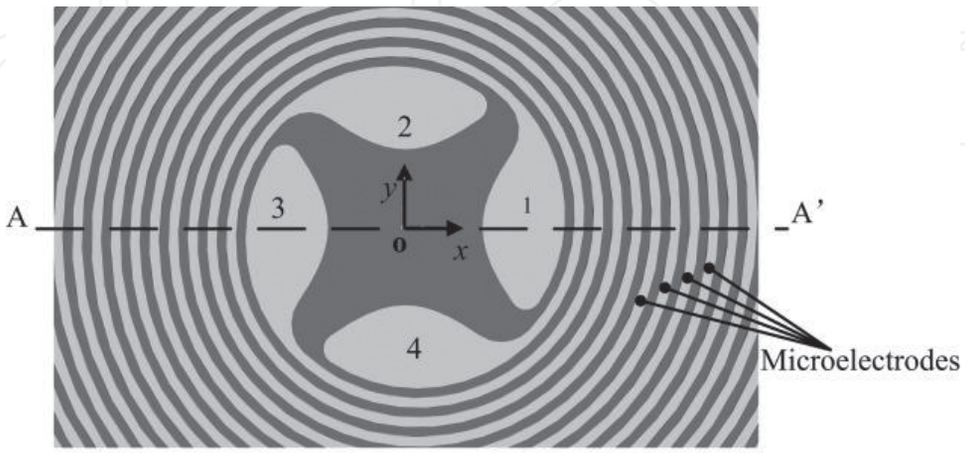

Figure 3. The enlarged drawing of quadrupole electrodes and spiral electrode bars with a width of 25 μm above the photoconductor. The coordinate system is shown, and the direction of z axis complies with right-handed screw rule [40].

layer and metal microelectrode layer were consecutively fabricated above the *a*-Si:H layer. The microfluidic chamber was designed and fabricated for suspending and manipulating particles. The photoconductor layer consisted of a 25–nm-thick insulating silicon nitride layer—to keep the insulation between the metal electrode layer and *a*-Si:H layer, a 1–2-μm-thick *a*-Si:H layer (include intrinsic *a*-Si:H layer and n + *a*-Si:H layer), and a bottom ITO conductive film (50 nm thick) in sequence. The potential of each successive signal could be set as phase shifted by a further multiple of 90° to produce quadrature signals or phases of 0°, 180°, 0°, 180° to produce traditional non-uniform field. It integrated metallic microelectrodes and the underneath photoconductive layer with LED-illuminating microspot.

The microelectrode layer contains of four parallel spiral electrodes as presented in **Figure 2**. When the four spiral electrode elements are energized with sinusoidal voltages with relative phase differences, a travelling electric field is generated and travels along the radial direction of the spiral array. A rotating electric field is also generated in the central free-space region denoted as central region. The spiral electrodes have the advantages of equivalent driving force to the particles at an arbitrary peripheral position. The quadrupole electrodes are located in the central area of spiral electrode array. The central region is surrounded by the quadrupole electrodes as shown in **Figure 3**. The geometrical shape of central region somewhat influences the distribution of the electric field around, and thus the sharp geometry should be avoided.

The experimental platform was established by assembling commercial optics, projector and an upright microscope. A digital micromirror device (DMD)-based projector (SHARP XG) was used as both the light source (via its dc lamp) and the interface between DMD driver circuit and the computer. The DMD forms a light image (or called optical pattern) according to the output signal of the PC's external monitor port. The optical image at the output of the projector lens was collimated, collected and reflected through the reflector at 45 degree to the horizontal and upward directed into a 10X driven lens from the lower location. The optical image was focused by the object lens and finally projected onto the photoconductive layer of ODEP device.

3. Manipulation modes and controlling regimes in FOD

3.1. Filtering

Usually, the impurities or non-target stuff (such as some types of microparticles) in the raw sample should be filtered firstly in the pre-treatment for the sample. The filtering experiment was implemented via an optical line scanning as shown in **Figure 4**. In the filtering experiment, with an applied 20 V_{pp} at 600 kHz, the normal pollen grains with diameters of 17–21 μm and most of the 30-μm diameter polystyrene particles were driven by the optical line with a width of ~70 μm from the upper area (**Figure 4a-b**) toward the bottom area of the view (**Figure 4c-d**). In contrast, the degenerative pollen grains and few polystyrene particles were left behind and stayed in their original positions. Therefore, the filtering function was able to be realized. This separation phenomenon is probably because the particles left behind were difficult to be polarized relative to the normal ones, which resulting in a much smaller DEP force for the abnormal ones. As long as the optical line velocity did not exceed the maximum synchronous velocity

http://dx.doi.org/10.5772/67928

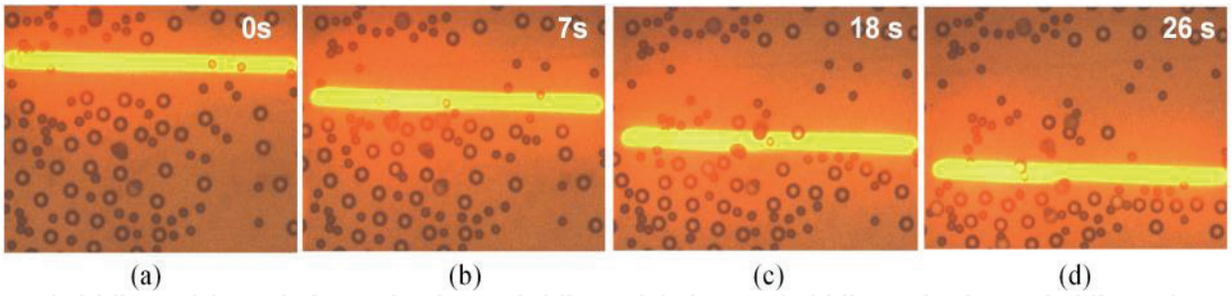

Figure 4. Snapshots of the filtering process in which a scanning light line moved from the top (a) to the bottom (d) of the viewing frame. Degenerative pollen grains and few polystyrene particles were left behind the optical line (b-d), while the normal particles were kinetically actuated by the scanning optical line.

(MS-velocity) of the normal particles [41] (i.e., maximum filtering velocity), the filtering function could be achieved. If the optical line velocity exceeded the MS-velocity, all particles would be left behind the scanning optical line, which made the filtering unavailable. This filtering experiment demonstrated the feasibility of the ODEP filtering.

3.2. Transporting

DEP can trap single particles and then transport the particles to desired positions, and the moving paths can be programed and controlled. As shown in, under the AC voltage of 20 V_{pp} and 1 MHz, two 30-μm diameter particles (**Figure 5a**) were trapped individually and moved along the programmed motion paths (two particles were marked by numbers 1 and 2 shown in **Figure 5**). These two particles were able to move simultaneously according to their own routings. The optical patterns can be controlled by the ODEP controlling software developed by our group. The polystyrene particles were always trapped by two optical rings those have an external diameter of ~150 μm and an interior diameter of ~40 μm during the transporting. Particle 1 and particle 2 kept moving and following the kinetic motion of the optical rings from the initial positions at the upper area (**Figure 5a**) to the lower area (**Figure 5h**) of the snapshot. The two particles moved simultaneously and always kept away from each other during the transporting, as shown in **Figures 5b–g** until they exchanged their positions and arrived at the terminative destinations.

3.3. Concentrating

In many biochemical applications, the reaction is very weak between a single bioparticle and other reagent, but a concentrated population of particles can react with other reagent intensively with much more obvious phenomena. Thus, when the raw sample was filtered and transported to the target locations, the selected particles would need concentration for the following detecting operations. The experiment presented in **Figure 6** serves as a typical example for presenting the concentrating regime of ODEP.

With an applied voltage of 20 V_{pp} at 800 kHz, at an arbitrary area (**Figure 6a**), the microlight pattern with a ring-shape can be used to collect a population of particles and can move the trapped particle population to an arbitrary location. The microparticles stayed inside the optical ring with a uniformly patterned array during the concentrating process (**Figure 6a-f**), and

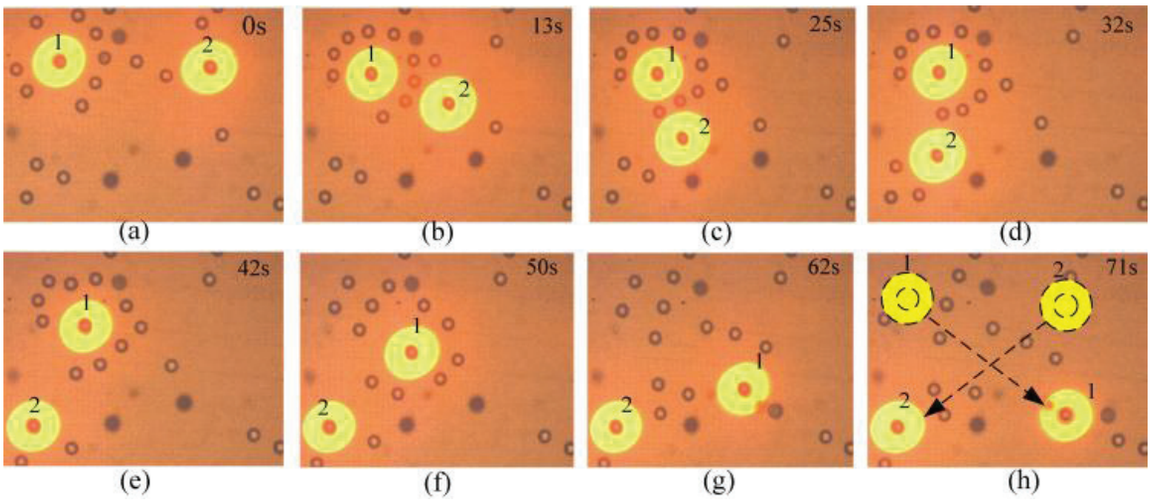

Figure 5. Snapshots of the transporting of two individual polystyrene particles parallelly. Particle 1 and particle 2 were driven from the upper area (a) toward the lower region (h) of the view field and the two particles switched their positions during the downward transporting process over time (c-g). The optical rings drawn by dashed lines in (h) indicate the original positions of the two particles [39].

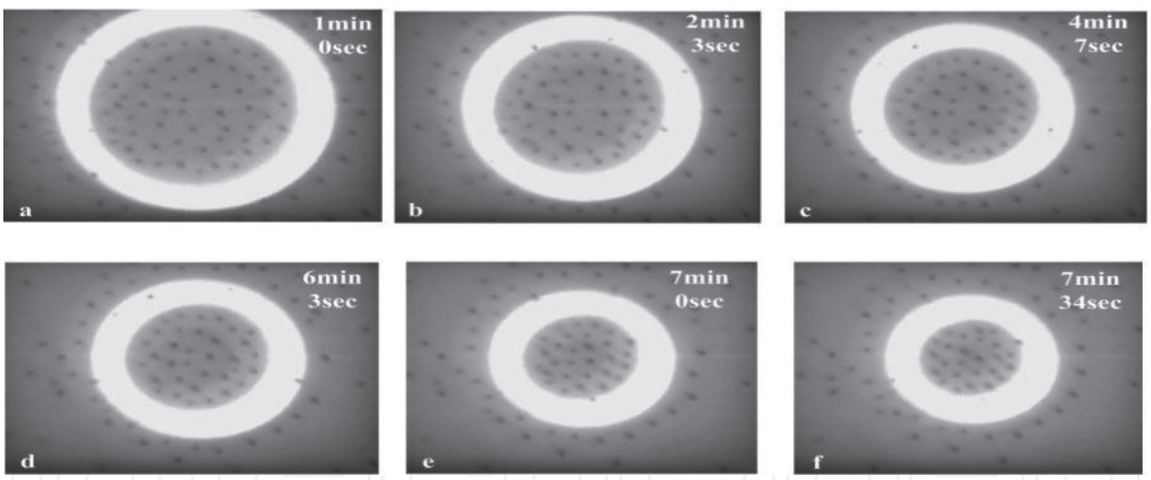

Figure 6. Concentration procedure for the microparticles with a diameter of 4 μm (20 Vpp, 800 kHz). (a) The initial distribution of microparticles. (b-e) The concentrating process of particles over time. (f) The final distribution of concentrated particles.

the distances between adjacent particles always kept the same. At this voltage magnitude, due to the dipole-to-dipole interaction between adjacent particles, the distance between adjacent particles is difficult to eliminate. The distances between particles were obviously larger than the particle diameter (**Figure 6**). If the voltage increased, the ODEP force would increase, which seems to drive the particles more concentrated. However, it is not that case when the voltage was larger than 20 V_{pp} in this experiment, because the increased voltage also enforced the interactional repelling force between particles.

http://dx.doi.org/10.5772/67928

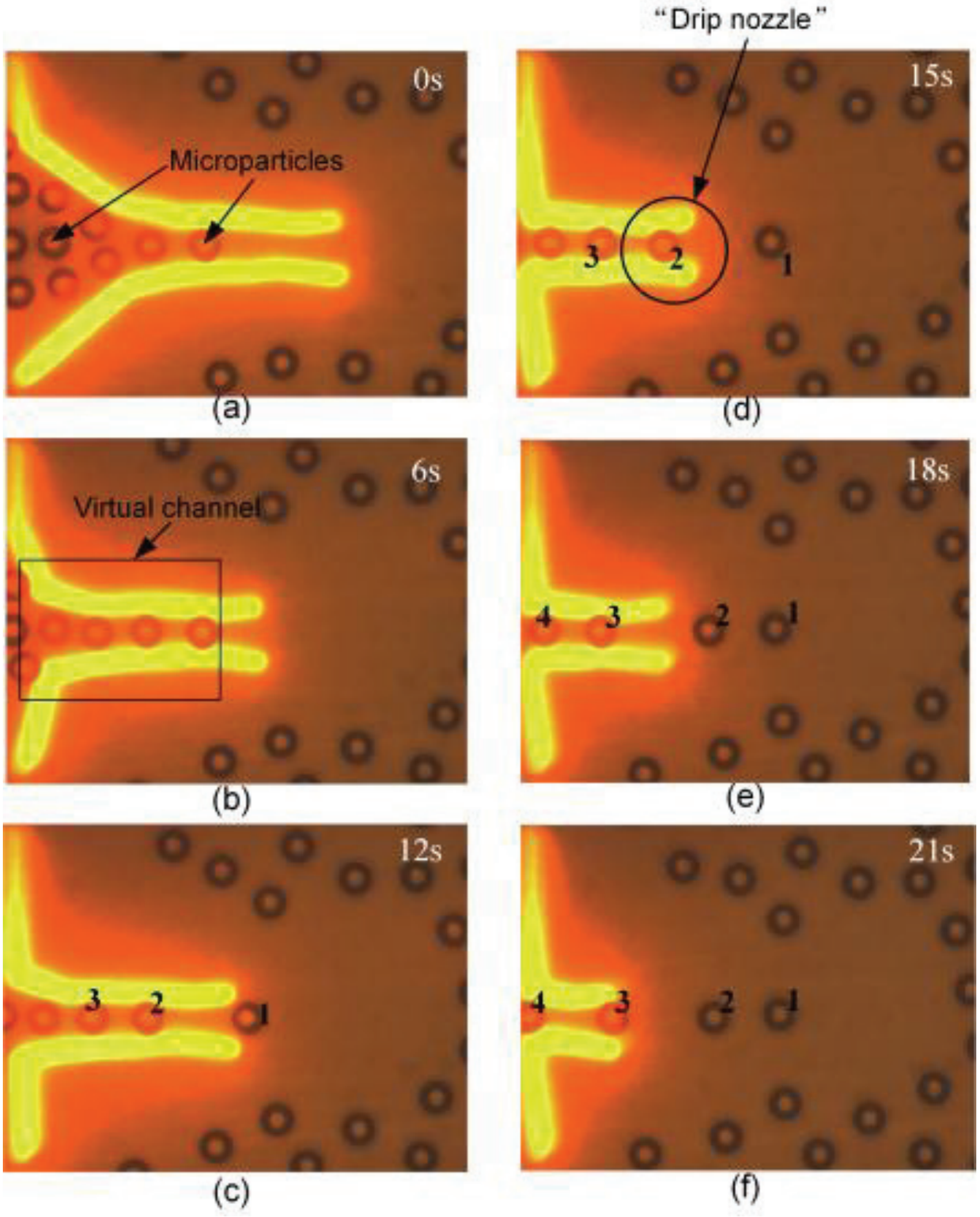

Figure 7. Microparticles are focused into a narrow particle line and ejected one-by-one by optical virtual channel and "drip nozzle." The micropattern projected onto the photoconductive layer to generate a negative ODEP force. Original state (a) is the initial spatial distribution of microparticles. While the optical virtual channel and "drip nozzle" deformed continuously, the random-located particles were gradually forming a straight particle line as shown in (b–d). Finally, the particles formed a linear array, and there were obvious spacing distances between particles as shown in (e–f).

3.4. Focusing

In many biochemical analyses, focusing is another important postprocessing mode apart from the procedures of concentrating particles. Focusing is mainly utilized to continuously and automatically count and detect individual particles. The ability to focus and eject particles based on ODEP is demonstrated in **Figure 7**.

In this study, a "drip nozzle" formed by the optical micropattern projected on the photoconductive layer was used to focus the microparticles in a straight sample flow and eject particles one by one. The optical lines forming the "drip nozzle" were set with a width of around the diameter of microparticles (**Figure 7**). The geometrical shape of optical pattern was real-time controlled so that the "drip nozzle" could continuously deform according to the current distribution of microparticles. The particles with 30-μm diameter moved out from the "drip nozzle" under the repelling ODEP force. This relative motion could also be regarded as the linear flow of particles relative to optical patterns. With an applied 24 V_{pp} at 600 kHz, the microparticles underwent negative ODEP force which always drove particles away from the virtual electrodes (optical micropattern) and thus kept particles horizontally swam in the virtual channel and then swam out of the "drip nozzle" accompany by the deformation of the optical virtual channel and "drip nozzle." Finally, the microparticles were focused into a straight particle line and had obvious spacing distances between particles 1 and 4 (**Figures 7e–f**). In this operation mode, there was no substantial fluidic flow to assist the focusing of the microparticles. The focusing efficiency grew when the optical line width increased but less than twice the particle diameter.

4. Manipulation of self-assembled microparticle chains by electroosmotic flow-assisted electrorotation in FOD

4.1. Background for microparticle chain manipulation

The microscopic particle chain is a common form of assembled particles, which involves in the colloidal, biological, electronic, photonic, magnetic fields. It plays an important role in these fields, as it serves as a link between the nanoscale world and meso- or macroscale objects. Currently, the methods for manipulating microparticle chains have become crucial for developing techniques on patterning magnetic nanoparticle arrays [42], forming regular superstructures by nanoparticles [43], constructing strings of particles [44], and creating multicellular assemblies [45] and live colloidosome structures [46]. In order to flexibly manipulate particle chains, various methods were developed, including the physical methods based on electric field, geometric constraint, dipole-dipole interactions or surface roughness direction [47] and the chemical methods based on linker molecules, oriented aggregation or non-uniform stabilizer distributions [34]. In this study, the formation and rotational manipulation of microparticle chains in real time are experimentally demonstrated by using optically induced electrorotation (OER) and ACEO flow in FOD.

http://dx.doi.org/10.5772/67928

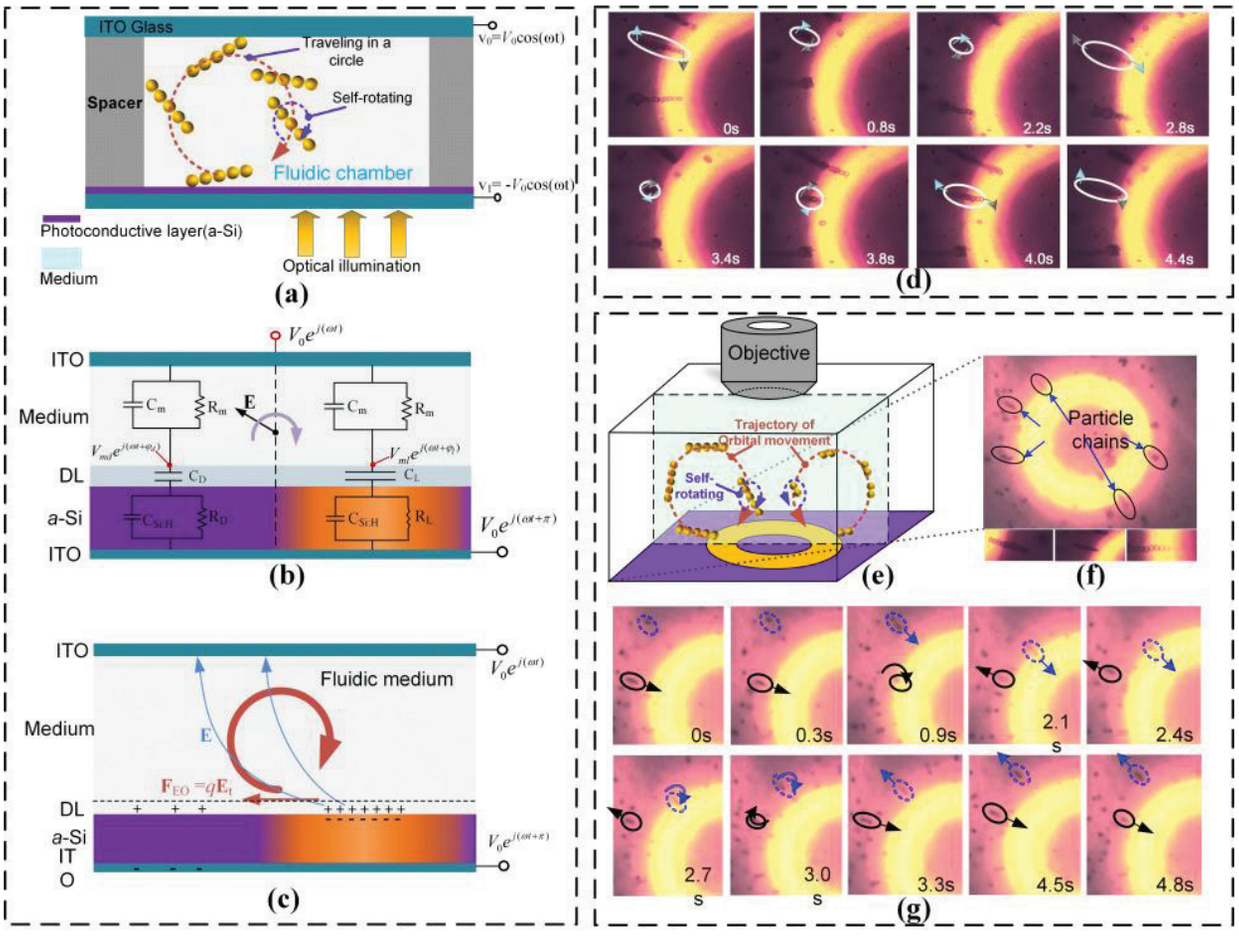

Figure 8. Schematically illustration of the OET device configuration and the principle for generating rotating electric field and ACEO flows. (a) Conceptual illustration of the self-rotation and circular travelling of an entire particle chains. The motion trajectories of the particle chain around the edge of illuminated area are indicated by dashed curve lines. (b) Device structure and mechanism for generating the rotating electric field around the border between dark and light regions. ω is the angular frequency, t is time, and V_0 is amplitude of AC voltage. (c) Electroosmotic fluid roll formed around the border between light and dark regions. (d–g) Experimental results of self-rotation and orbital travelling of an entire particle chains [48].

4.2. Experiment setup and working principle

The structure of the OET device and the scheme for rotating particle chains are conceptually illustrated in **Figure 8**. The equivalent circuit of the OET device is shown in **Figure 8b**. The device is composed by the upper and lower indium tin oxide (ITO) slides, photoconductive layer (hydrogenated amorphous silicon, *a*-Si:H) with a thickness of t_a and a relative permittivity ε_{ar}, and a fluidic chamber with a height of t_m and the applied AC voltages. The electrical conductivity of the photoconductor layer at unilluminated and illuminated areas is denoted as σ_{al} and σ_{ad}, respectively. The microfluidic chamber contains fluidic medium with a relative permittivity ε_{mr} and an electrical conductivity of σ_m. The micro-particles are suspended uniformly in the fluidic chamber at the initial time. The potentials applied at the upper and lower ITO layers.

The principle of the light-dark binary image induced rotating electric field (e-field) is indicated in **Figure 8a–b**. The a-Si:H layer has different impedances on light and dark sides, which leads to the amplitude and phase difference in the electric potentials at upper surface ($V_0 e^{j\omega t}$), photoconductive layer/medium interface in light area ($V_{ml} e^{j(\omega t+\phi_l)}$) and dark area ($V_{md} e^{j(\omega t+\phi_l)}$). In a particular frequency range, these three AC potentials can create a rotating e-field in fluidic medium around the border between light and dark regions, which will lead to self-rotating of the one-dimensional particle chains due to the interaction between the dipole moment of particle chain and rotating e-field.

According to equivalent circuit of the OET device shown in **Figure 8b**, and assuming that the impedance of conjunction between the light and dark regions in the a-Si:H layers is very large indicating no current flows across the border, the potential phasor at the bottom surface of fluidic chamber denoted as Φ_i is given by

$$\Phi_i = V_0 e^{j\omega t}\left(\frac{Z_a + Z_{DL} - Z_m}{Z_a + Z_{DL} + Z_m}\right) = V_{mi} e^{j(\omega t+\varphi_i)} \tag{3}$$

In (3), the subscript i in voltage amplitude V_{mi} and initial phase φ_i and can be replaced by "l" or "d" indicating the light or dark condition for the optical projection onto photoconductor, respectively. The impedance of photoconductor per unit area at light and dark regions is, respectively, expressed as follows

$$Z_{a\_l} = \frac{R_{a\_l}}{1 + j\omega C_a R_{a\_l}} \tag{4}$$

$$Z_{a\_d} = \frac{R_{a\_d}}{1 + j\omega C_a R_{a\_d}} \tag{5}$$

Here, the $C_a\left(=\varepsilon_{ar}\varepsilon_0/t_a\right)$ is the capacitance of a-Si:H layer per unit area, $R_{a\_l} = t_a/\sigma_{al}$ and $R_{a\_d} = t_a/\sigma_{ad}$ are the resistances of illuminated and unilluminated a-Si:H layer per unit area, respectively. Here, the double layer (DL) forms at medium/a-Si:H interface due to the interfacial polarization as shown in **Figure 8b**. The characteristic thickness of DL (t_{DL}) can be estimated by Debye length [38]. The detailed information could be found in Ref. [49]. The microparticle chain can be self-assembled under an e-field **E**, and then, a polarization could be induced in the particle chain. The effective dipole of the entire particle chain (denoted as **P**c) forms after the establishment of the field **E** with a time delay, because it takes finite time for the dipole moment to completely form. When the e-field **E** rotates, **P**c will follow it and rotates with a phase lag. The particle chain experiences a rotational torque as follows [50, 51],

$$\Gamma = \frac{1}{2}\mathrm{Re}[\,\mathbf{P}_c \times \mathbf{E}^*\,] \tag{6}$$

where $\mathbf{P}_C$ is the complex phasor of the effective dipole moment of a particle chain, and E^* is conjugated complex phasor of the e-field acting on particle chains. More information on effective dipole moment of a particle chain could be found in Refs. [49, 52].

ACEO flow is also induced at appropriate frequencies in the OET or ODEP device. ACEO flow is the motion of fluid due to an interaction between an e-field and the DL induced at medium/a-Si:H interface as shown in **Figure 8c**. The tangential e-field mainly arises around the edges of optical micropatterns. Therefore, the ACEO flow mainly occurs around the optical micropatterns projected on the photoconductive layer. ACEO flow lets the particle chains traveling in a nearly circular trajectory as shown in **Figure 8c**. After applying the voltage,

counterions accumulate in the DL mainly within the illuminated region. Due to the distortion of electrical field induced by the optical pattern, a tangential component of e-field arises round the medium/a-Si:H interface. As a result, the ions in DL are subjected to the tangential electrostatic force along the a-Si:H surface. This force is then transmitted to the fluid and drive the boundary liquid to flow with a slip time-averaged velocity that can be calculated by using the Helmholtz–Smoluchowski equation as in Refs. [53, 54]

$$\langle u_{EO} \rangle = -\frac{1}{2}\frac{\varepsilon_{mr}\varepsilon_0}{\eta_b}\mathrm{Re}\left[(\boldsymbol{\varphi}-\boldsymbol{\varphi}_s)(-\tilde{\mathbf{E}}_t^{\,*})\right], \tag{7}$$

where $\boldsymbol{\phi}$ is the potential phasor just outside the DL, $\boldsymbol{\phi}_s$ is the potential at the non-slip plane close to the solid surface of the DL. $\tilde{E}_t^*$ is the conjugated complex phasor of the tangential e-field just outside the DL. η_b is dynamic viscosity of the bulk solvent. $\eta_b = 1 \times 10^{-3}$ Pa·is for aqueous medium. The electrorotation of particle chains can be solely operated at relative higher frequencies because the ACEO flow decreases significantly at higher frequencies. Appropriately tuning down the frequency can make the ACEO flow available and then assist the self-rotating particle chains to travel along circled trajectory.

In experiment, the polystyrene (PS) microparticles did not form particle chains with a low voltage, but would start to form particle chains when the voltage increases to a threshold value. The PS particles with a diameter of 4 μm self-assembled into chains within the fluidic medium when the applied voltage was increased to 15 V_{pp}. The kinetic motion of particle chains could be enhanced with the increased voltage until 28 V_{pp}. The self-rotation of particle chain around its geometric center was obtained inside fluidic medium at 700 kHz because the ACEO flow can approximately be dismissed at these relatively higher frequencies. As shown in **Figure 8d**, the two ends of particle chains exchanged their positions after 2.8 s and had accomplished the first half-cycle of the rotation. Then, the particle chains continued to self-rotate through the other half-cycle, and it took only 1.6 s. The rotation rate of particle chain varied with time within a single period.

At lower frequencies, the particle chains circularly travelled around the center of fluid roll generated by the optically induced ACEO effect. As indicated in **Figure 8e**, the ACEO flow assisted particle chain rotation can be decomposed into two component motions: the self-rotation and orbital movement of the entire particle chain. **Figure 8f** shows the optically projected ring-shaped micropattern and the formed microparticle chains around the optical ring. The ACEO flow assisted microparticle chain rotation at 480 kHz is shown in **Figure 8g**. The particle chains were moving closer to the edge of optical pattern and turned around through the vertical planes after a short time (less than one second or a few seconds). Then, the particle chains were moving away from the optical ring along the circular path. They continued to turn around at the other corner of the circular path and then moved closer to optical ring again. The orbital moving of particle chains was not uniform motion and the vertical plane in which the circularly orbital movement occurred was approximate parallel to the diametrical dimension of optical ring. The complex movement of particle chains exhibited a three-dimensional (3D) movement of distributed particle chains that had more degrees of freedom than the 2D motion. These results offer more opportunities for spatially controlling the position, posture and orientation of particle chains for the applications regarding electrics, mechanics, optics and biodevices.

5. Manipulation of microparticles in a prototypical HOD

5.1. Integrated design and fabrication of metal electrode array and photoconductive layer

The virtual electrode is actually the microlight image in which we project in vertical direction on the photoconductive layer. It can precisely locate single microparticles and dynamically drive them. On the silicon nitride layer, we fabricated the planar microelectrode structure by photolithography. The microlight pattern could be designed according to specific experimental or application requirement, and it may be, for example, a linear or a spiral microelectrode array. In practical operations, we usually imposed low voltage to prevent insulating layer from breaking down by strong electric field. The spacer to mechanically support the fluidic chamber can be fabricated by polydimethylsiloxane (PDMS) or just double-sided tapes. The electric pads of microelectrodes were led out and connected to external PCB by gold wires. Then, the connectors on PCB were further connected to the external signal generator. The HODs were finally fabricated as shown in **Figure 9**.

The microelectrode array was fabricated by the depositing about 2000nm-thick layer of aluminum or gold on top of the insulating layer through electron beam evaporation. Then, the spiral pattern (**Figure 9**) was produced by standard or "lift-off" lithography process. In the standard lithography process, the corrosion rate needs to be strictly controlled in order to prevent possible damage to the insulating layer as well as the photoconductive layer. In our study, we had also sputtered gold over the silicon carbide layer (insulating layer) and then fabricated microelectrodes. Sputtering process and standard lithography process had a certain impact on the layer-to-layer electrical connections. In general, after the deposition by electron beam evaporations, the insulating property between the aluminum layer and the substrate is better. This usually could meet the insulating requirement of layers in this device. On the other hand, depositing gold by sputtering method onto the photoconductive film usually involved a relatively higher sputtering power or higher temperature in vacuum chamber (typically the sputtering involved a much higher temperature than the electron beam evaporation). These process features may result in that the *a*-Si:H layer was locally damaged within very tiny scale, which may enhance the partial defects in the thin film. More importantly,

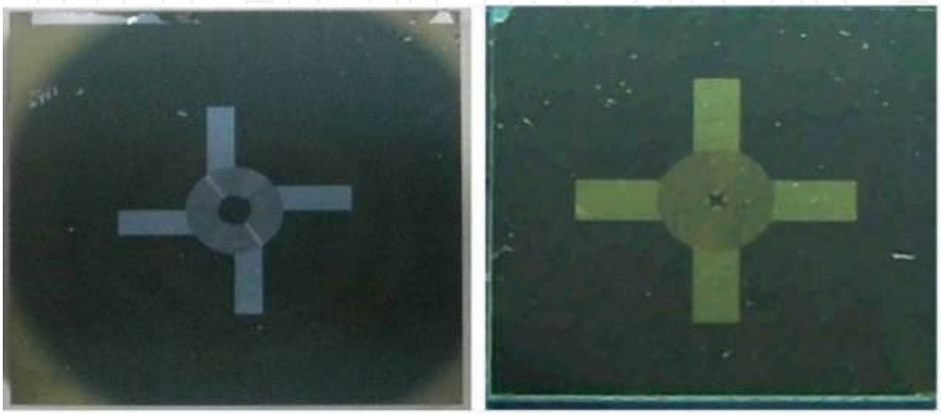

Figure 9. The prototypical photos of the substrates with metal microelectrodes and photoconductive layers for HOD.

http://dx.doi.org/10.5772/67928

the sputtering process also could form the Schottky contact between the metal layer and the below semiconductor layers. Consequently, the time-averaged magnitude of local AC impedance between the metal layer and bottom ITO layer was smaller. The measurement results showed a low resistance of a few hundred ohms to thousands of ohms between the metal layer and the bottom ITO layer.

5.2. Experiment result of the distribution of particles when light pattern is off

In this experiment, a 10 V peak-to-peak (V_{pp}) AC bias with a frequency of 1 MHz is applied between the top and bottom ITO electrodes, and the light pattern is not projected onto the HOD. The metal electrodes might be connected to the bottom ITO layer by a very low resistance through the Schottky contact between the metal and photoconductive layer and/or through the local defects of *a*-Si:H layer, when the AC voltage was applied. Therefore, most of the applied voltage drops across the liquid layer (for the resistance between the metal electrodes, and bottom ITO electrode is very small). However, in the gap region between the metal electrodes, most of the voltage drops across the photoconductive layer, only minority of the voltage drops across the liquid layer. Therefore, most of the particles moved to the gap region between metal electrodes by the negative DEP, as the white dotted circles indicated in **Figure 10A** and **B**. In addition, a few particles remained on the metal electrodes, as shown in **Figure 10A**. The single particle on metal electrode was initially near the center region of the metal electrodes where the DEP is very small, and it was already under the balanced state from the very beginning. That is why it remained on the electrodes instead of being driven to the gap region. The Schottky contact formed at the interface of the gold layer and photoconductive layer, the electrons flew from the photoconductive layer to the metallic layer. It enhanced the short connection effect between the bottom ITO film and the metal electrodes.

5.3. Experiment result of the particle's assembly under the assistance of light pattern

Before the microlight pattern was projected onto the HOD, the particles had distributed along the trend of spiral electrodes (**Figure 10**). The particles could be actuated by moving the microlight pattern when the light pattern (the diameter was nearly 120μm in this experiment)

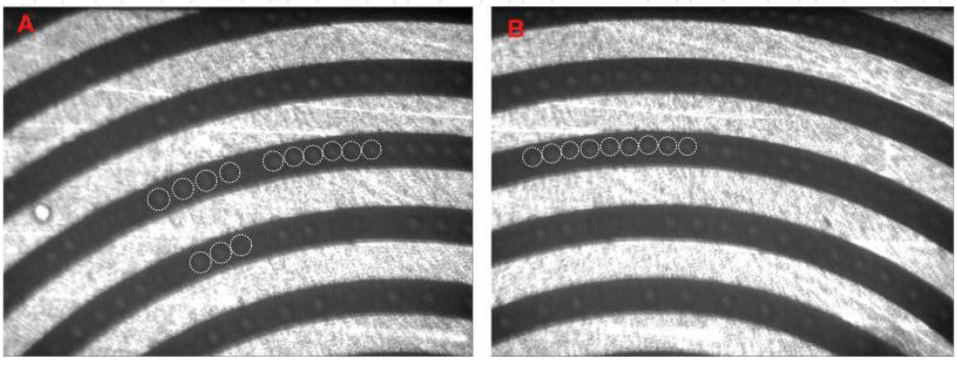

Figure 10. Generation and distribution of particle array or chains when ac voltage (10 Vpp, 1 MHz) was applied between the top and bottom ITO layers. (A) The arrayed microparticles in the gap of electrodes and a few ones on the metal electrodes. (B) The arrayed microparticles all in the gap of electrodes. The metallic electrode array was not energized by external voltages. Particles diameter is 10 μm. The widths of the electrodes and gap are both 20 μm.

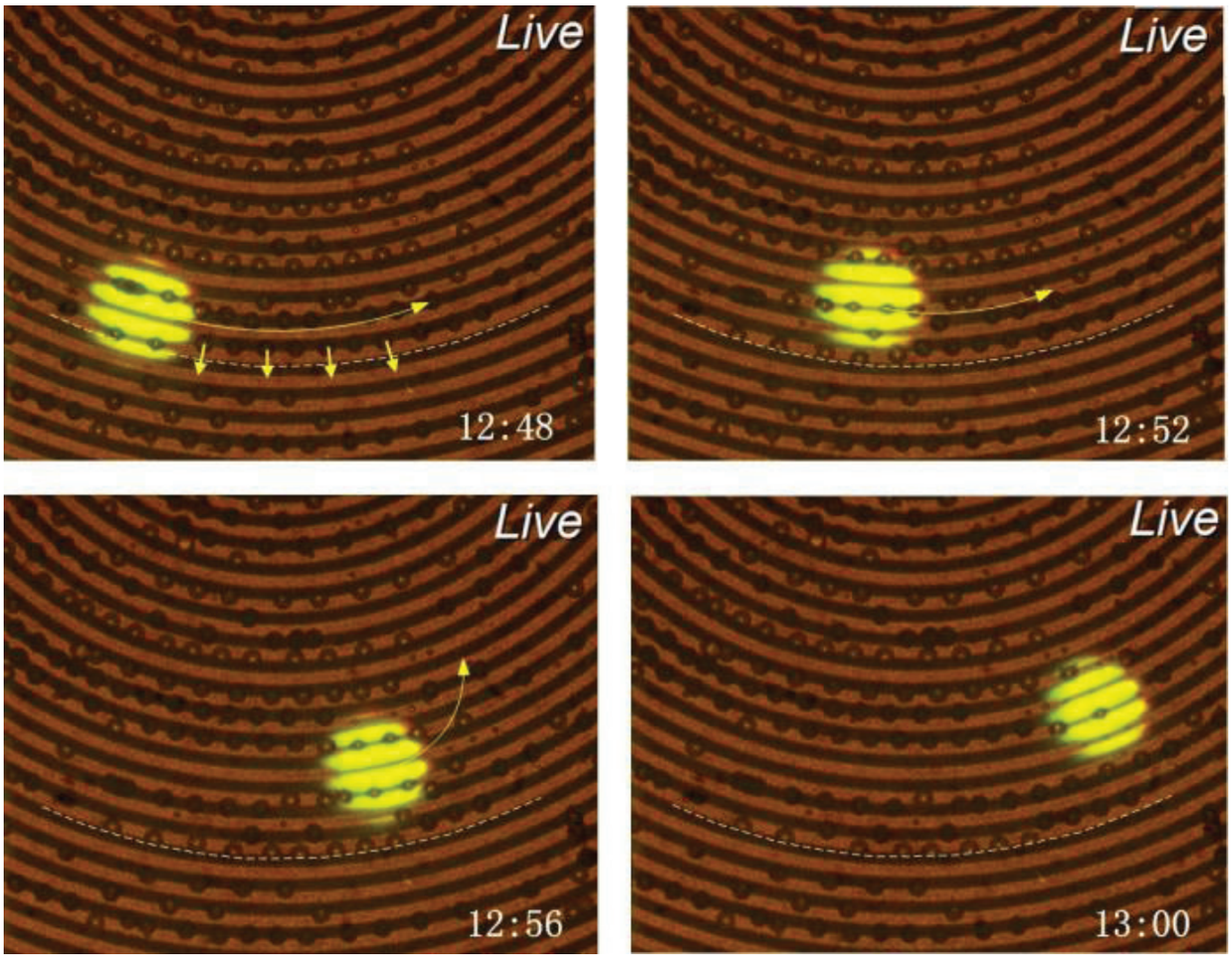

Figure 11. Particle manipulation in typical HOD. The curve arrow indicated the moving track of the light spot. Particles along spiral electrode and away from the white dotted arc were gradually moving closer to the position marked by the dotted arc due to the repulsive force from the light spot. The AC voltage between the top and bottom ITO layers is 5 V_{PP} and 1 M Hz. The particle diameter was 30 μm, and the widths of the electrode and gap were both 20 μm.

was projected as shown in **Figure 11**. The light pattern produced by LED can meet the needs of the power for operation. The spatial interval between the particles can be manipulated by adjusting the magnitude of the voltage applied between the upper and lower ITO layers, and the increase in voltage leads to larger separation between the particles. The metallic electrode array was not electrically energized. As shown in **Figure 11**, the DEP forces acting on microparticles were generated due to the participation of both the planar metal electrodes and microlight pattern in the electric field generated by the voltage applied between the upper and lower ITO layers. The curve arrow indicated the moving track of the light spot. Particles along spiral electrode and away from the white dotted arc were gradually moving closer to the position marked by the dotted arc due to the repulsive force from the light spot. This HOD can meet the need of the large-scale particles manipulation requiring the particles to form specific geometrical array. In this device, incorporation of metal microelectrode array was more suitable for the situation that the required separation between particles was small, and the tracks of particle distribution are more elaborate than the virtual electrode produced by light projection system. That is because microlight pattern needs to be produced by using

http://dx.doi.org/10.5772/67928

even more complex and higher cost optical device, and the Gaussian distribution of light pattern border, the diffraction and the scattering may also limit the light pattern to have the smaller, finer and sharper geometry. This combination of metal microelectrode and light-induced virtual electrode in HOD is appropriate for the situation that the area for arranging particles is compact, and the particular geometric form (like curve shape distribution) is expected. This technique may also have the potential for manipulating large number of cells and be incorporated into the self-organization scheme for constructing multicellular structure [55, 56], in order to develop biomaterials applied in regenerative medicine.

6. Summary

In this chapter, *firstly*, the design and fabrication of flat optoelectronic devices (FOD) and hybrid optoelectronic device (HOD) were elucidated. *Secondly*, the scanning filtering, multiparticle parallel transportation, particle concentration and the focusing for single particle queue were experimentally demonstrated and analyzed. *Thirdly*, the self-electrorotation and circularly orbital movement of the microparticle chains in real time are experimentally demonstrated by FOD. The rotating electrical field for implementing the optically induced electrorotation (OER) of particle chains can be generated by utilizing the different impedances of photoconductor layer at light and dark areas. The optically induced ACEO flow was simultaneously produced accompanying the OER effect. This non-contact manipulation method for rotating particle chains has the potential for spatially regulating the posture, orientation and position of microparticle chains or microstructures. *Fourthly*, The hybrid device HOD enables rapid large-scale patterning and locally position adjustment of single microparticles. This technique makes up the shortcoming of lacking flexibility possessed by metallic microelectrodes and takes advantages of both electrode-based DEP and microimage-based DEP technologies.

Acknowledgements

This work was supported by grants from the National Natural Science Foundation of China (51505127), the Natural Science Foundation of Jiangsu Province (BK20161197), the Changzhou Sci&Tech Program (CE20165029), and the Fundamental Research Funds for the Central Universities of China (2015B04414). Parts of this chapter are reproduced from authors' recent conference publication [40, 48].

Author details

Xiaolu Zhu* and Yifei Yang

*Address all correspondence to: zhuxiaolu@hhu.edu.cn

College of Mechanical and Electrical Engineering, Hohai University, China

References

[1] Medoro G, Nastruzzi C, Guerrieri R, Gambari R, and Manaresi N. Lab on a chip for live-cell manipulation. IEEE Design & Test of Computers. 2007; 24(1): 26-36.

[2] Vahey MD and Voldman J. An equilibrium method for continuous-flow cell sorting using dielectrophoresis. Analytical Chemistry. 2008; 80(9): 3135-3143.

[3] Wang X-B, Huang Y, Gascoyne PRC, and Becker FF. Dielectrophoretic manipulation of particles. IEEE Transactions on Industry Applications. 1997; 33(3): 660-669.

[4] Gascoyne PRC and Vykoukal JV. Dielectrophoresis-based sample handling in general-purpose programmable diagnostic instruments. Proceedings of the IEEE. 2004; 92(1): 22-42.

[5] Small WR, Stoyanov SD, and Paunov VN. Scaffold free fabrication of linear multicellular assemblies by dielectrophoretic hydrogel trapping technique. Biomaterials Science. 2013; 1(9): 996-1002.

[6] Flanagan LA, Lu J, Wang L, Marchenko SA, Jeon NL, Lee AP, and Monuki ES. Unique dielectric properties distinguish stem cells and their differentiated progeny. Stem Cells. 2008; 26(3): 656-65.

[7] Iliescu C, Tresset G, and Xu G. Dielectrophoretic field-flow method for separating particle populations in a chip with asymmetric electrodes. Biomicrofluidics. 2009; 3(4): 044104-10.

[8] Eguchi M, Imasato H, Yamakawa T, and Ieee, Separation of blood cells by employing dielectrophoresis and traveling-wave electric fields. 2012 World Automation Congress; 2012.

[9] Schonfeld F, Griebel A, Konrad R, Rink S, and Karlsen F. Development of a [mu]-concentrator using dielectrophoretic forces. Journal of the Association for Laboratory Automation. 2002; 7(6): 130-134.

[10] Yokokawa R, Manta Y, Namura M, Takizawa Y, Le NCH, and Sugiyama S. Individual evaluation of DEP, EP and AC-EOF effects on lambda DNA molecules in a DNA concentrator. Sensors and Actuators B-Chemical. 2010; 143(2): 769-775.

[11] Cheng IF, Chang HC, Chen TY, Hu CM, and Yang FL. Rapid (<5 min) identification of pathogen in human blood by electrokinetic concentration and surface-enhanced raman spectroscopy. Scientific Reports. 2013; 3: 2365. DOI: 10.1038/srep02365

[12] Crews N, Darabi J, Voglewede P, Guo F, and Bayoumi A. An analysis of interdigitated electrode geometry for dielectrophoretic particle transport in micro-fluidics. Sensors and Actuators B: Chemical. 2007; 125(2): 672-679.

[13] Dos Santos MVP, Lima LPB, Mayer RA, Beron F, Pirota KR, and Diniz JA. Dielectrophoretic manipulation of individual nickel nanowires for electrical transport measurements. Journal of Vacuum Science & Technology B. 2015; 33(3): 031804.

[14] Hossan MR, Dutta P, Dillon R, and ASME. Numerical investigation of DC dielectrophoretic particle transport. ASME Fluids Engineering Division Summer Meeting—2014, Vol 2: Fora; 2014.

[15] Fu LM, Yang RJ, Lin CH, Pan YJ, and Lee GB. Electrokinetically driven micro flow cytometers with integrated fiber optics for on-line cell/particle detection. Analytica Chimica Acta. 2004; 507(1): 163-169.

[16] Yao B, Luo GA, Feng X, Wang W, Chen LX, and Wang YM. A microfluidic device based on gravity and electric force driving for flow cytometry and fluorescence activated cell sorting. Lab on a Chip. 2004; 4(6): 603-607.

[17] Jamshidi A, Pauzauskie PJ, Schuck PJ, Ohta AT, Chiou PY, Chou J, Yang PD, and Wu MC. Dynamic manipulation and separation of individual semiconducting and metallic nanowires. Nature Photonics. 2008; 2(2): 85-89.

[18] Chiou PY, Ohta AT, and Wu MC. Massively parallel manipulation of single cells and microparticles using optical images. Nature. 2005; 436(7049): 370-372.

[19] Tsutsui H and Ho CM. Cell separation by non-inertial force fields in microfluidic systems. Mechanics Research Communications. 2009; 36(1): 92-103.

[20] Cheng IF, Chang HC, Hou D, and Chang HC. An integrated dielectrophoretic chip for continuous bioparticle filtering, focusing, sorting, trapping, and detecting. Biomicrofluidics. 2007; 1(2): 021503.

[21] Hawkins BG, Smith AE, Syed YA, and Kirby BJ. Continuous-flow particle separation by 3D insulative dielectrophoresis using coherently shaped, dc-biased, ac electric fields. Analytical Chemistry. 2007; 79(19): 7291-7300.

[22] Yeo WH, Lee HB, Kim JH, Lee KH, and Chung JH. Nanotip analysis for dielectrophoretic concentration of nanosized viral particles. Nanotechnology. 2013; 24(18):185502. DOI: 10.1088/0957-4484/24/18/185502

[23] Maruyama H, Kotani K, Masuda T, Honda A, Takahata T, and Arai F. Nanomanipulation of single influenza virus using dielectrophoretic concentration and optical tweezers for single virus infection to a specific cell on a microfluidic chip. Microfluidics and Nanofluidics. 2011; 10(5): 1109-1117.

[24] Cho YK, Kim TH, and Lee JG. On-chip concentration of bacteria using a 3D dielectrophoretic chip and subsequent laser-based DNA extraction in the same chip. Journal of Micromechanics and Microengineering. 2010; 20(6): 1023-1035.

[25] Sen AK and Sajeesh P. Electrokinetic transport and separation of droplets in a microchannel. Microfluidics and Nanofluidics. 2014; 17(1): 97-106.

[26] Wang CH, Wang XZ, and Jiang ZD. Dielectrophoretic driving of blood cells in a microchannel. Biotechnology & Biotechnological Equipment. 2011; 25(2): 2405-2411.

[27] Khoshmanesh K, Nahavandi S, Baratchi S, Mitchell A, and Kalantar-Zadeh K. Dielectrophoretic platforms for bio-microfluidic systems. Biosensors & Bioelectronics. 2011; 26(5): 1800-1814.

[28] Zhang JM, Aguirre-Pablo AA, Li EQ, Buttner U, and Thoroddsen ST. Droplet generation in cross-flow for cost-effective 3D-printed "plug-and-play" microfluidic devices. RSC Advances. 2016; 6(84): 81120-81129.

[29] Pittermannova A, Ruberova Z, Zadrazil A, Bremond N, Bibette J, and Stepanek F. Microfluidic fabrication of composite hydrogel microparticles in the size range of blood cells. RSC Advances. 2016; 6(105): 103532-103540.

[30] Song YX, Wang CF, Li MQ, Pan XX, and Li DQ. Focusing particles by induced charge electrokinetic flow in a microchannel. Electrophoresis. 2016; 37(4): 666-675.

[31] Li D, Lu XY, Song YX, Wang JS, Li DQ, and Xuan XC. Sheathless electrokinetic particle separation in a bifurcating microchannel. Biomicrofluidics. 2016; 10(5): 1-13.

[32] Park S, Pan C, Wu T-H, Kloss C, Kalim S, Callahan CE, Teitell M, and Chiou EPY. Floating electrode optoelectronic tweezers: light-driven dielectrophoretic droplet manipulation in electrically insulating oil medium. Applied Physics Letters. 2008; 92(15): 151101.

[33] Hwang H, Lee D-H, Choi W, and Park J-K. Enhanced discrimination of normal oocytes using optically induced pulling-up dielectrophoretic force. Biomicrofluidics. 2009; 3(1): 14103.

[34] Kitching H, Shiers MJ, Kenyon AJ, and Parkin IP. Self-assembly of metallic nanoparticles into one dimensional arrays. Journal of Materials Chemistry A. 2013; 1(24): 6985-6999.

[35] Hwang H and Park JK. Optoelectrofluidic platforms for chemistry and biology. Lab Chip. 2011; 11(1): 33-47.

[36] Zhu XL, Yin ZF, and Ni ZH. Dynamics simulation of positioning and assembling multi-microparticles utilizing optoelectronic tweezers. Microfluidics and Nanofluidics. 2012; 12(1-4): 529-544.

[37] Yang YJ, Mao YF, Shin KS, Chui CO, and Chiou PY. Self-locking optoelectronic tweezers for single-cell and microparticle manipulation across a large area in high conductivity media. Scientific Reports. 2016; 6: 22630. DOI: 10.1038/srep22630

[38] Morgan H and Green NG. AC electrokinetics: colloids and nanoparticles. Micro-technologies and Microsystems Series, 2. 2003, Philadelphia, PA: Research Studies Press.

[39] Zhu XL, Yin ZF, Gao ZQ, and Ni ZH. Experimental study on filtering, transporting, concentrating and focusing of microparticles based on optically induced dielectrophoresis. Science China-Technological Sciences. 2010; 53(9): 2388-2396.

[40] Zhu XL, Yi H, Ni ZH, and IEEE. Novel design of multiphase optoelectronic microfluidic device for dielectric characterization of single biological or colloidal particles. 2009 ICME International Conference on Complex Medical Engineering. 2009. 542-547.

[41] Zhu XL, Yi H, and Ni ZH. Frequency-dependent behaviors of individual microscopic particles in an optically induced dielectrophoresis device. Biomicrofluidics. 2010; 4(1) :013202. DOI:10.1063/1.3279788

[42] Schelhas LT, Farrell RA, Halim U, and Tolbert SH. Directed self-assembly as a route to ferromagnetic and superparamagnetic nanoparticle arrays. Advanced Functional Materials. 2014; 24(44): 6956-6962.

[43] Zhou F, Xie MX, and Chen DY. Structure and ultrasonic sensitivity of the superparticles formed by self-assembly of single chain janus nanoparticles. Macromolecules. 2014; 47(1): 365-372.

[44] Termonia Y. Entropy-driven self-assembly of nanoparticles into strings. Colloids and Surfaces A: Physicochemical and Engineering Aspects. 2014; 447: 23-27.

[45] Brandy M-L, Cayre OJ, Fakhrullin RF, Velev OD, and Paunov VN. Directed assembly of yeast cells into living yeastosomes by microbubble templating. Soft Matter. 2010; 6(15): 3494-3498.

[46] Fakhrullin RF, Brandy M-L, Cayre OJ, Velev OD, and Paunov VN. Live celloidosome structures based on the assembly of individual cells by colloid interactions. Physical Chemistry Chemical Physics. 2010; 12(38): 11912-11922.

[47] Kraft DJ, Ni R, Smallenburg F, Hermes M, Yoon K, Weitz DA, van Blaaderen A, Groenewold J, Dijkstra M, and Kegel WK. Surface roughness directed self-assembly of patchy particles into colloidal micelles. Proceedings of the National Academy of Sciences of the United States of America. 2012; 109(27): 10787-10792.

[48] Zhu X. Electroosmotic flow assisted rotation of self-assembled microparticle chains using optoelectronic tweezers. in IEEE International Conference on Nano/micro Engineered and Molecular Systems. 2015.

[49] Zhu X. Manipulation of self-assembled microparticle chains by electroosmotic flow assisted electrorotation in an optoelectronic device. Micromachines. 2015; 6(9): 1387-1405.

[50] Jones TB. Electromechanics of Particles. 1995, New York: Cambridge University Press.

[51] Jones TB. Basic theory of dielectrophoresis and electrorotation. IEEE Engineering in Medicine and Biology Magazine. 2003; 22(6): 33-42.

[52] Jiang ZH, He XD, Han JC, Zhang BM, and Du SY. Fractal characterization of the dipole moments of dielectric particle chains. Journal of Electrostatics. 1998; 44(1-2): 47-51.

[53] Ramos A, Morgan H, Green NG, Gonzalez A, and Castellanos A. Pumping of liquids with traveling-wave electroosmosis. Journal of Applied Physics. 2005; 97(8): 084906.

[54] Lyklema J. Fundamentals of Interface and Colloid Science, Volume II: Solid–Liquid Interfaces. Vol. 2. New York: Academic Press; 1995.

[55] Zhu X, Gojgini S, Chen T-H, Teng F, Fei P, Dong S, Segura T, and Ho C-M. Three dimensional tubular structure self-assembled by vascular mesenchymal cells at stiffness interfaces of hydrogels. Biomedicine & Pharmacotherapy. 2016; 83: 1203-1211.

[56] Zhu X and Yang H. In-silico constructing three-dimensional hollow structure via self-organization of vascular mesenchymal cells. in *The 16th International Conference on Nanotechnology (IEEE NANO 2016)*. 2016. Sendai, Japan: IEEE.

IntechOpen